

Hydromagnetic Nanofluid Flow over an Exponentially Stretching Sheet in the Presence of Radiation and Nonuniform Heat Generation/Absorption

Emeka Amos¹ and Uchenna Awucha Uka^{2,*}

*Corresponding Author: ukau@babcock.edu.ng

¹ Department of Mathematics, Rivers State University, Port Harcourt, Nigeria.

² Department of Basic Sciences, Babcock University, Ilishan-Remo, Nigeria.

Abstract

The problem of hydromagnetic nanofluid flow in the presence of radiation and non-uniform heat generation/absorption past an exponentially stretching sheet is modeled in this study. By using similarity transformation, the equations of the flow are transformed to nonlinear coupled differential equations. The equations are then solved by the method of asymptotic series and the various flow profiles for the parameters governing the flow were obtained using the software "Mathematica Version 10". It is observed that increase in the magnetic field and radiation parameters lead to decrease in the velocity, while increase in the stretching sheet parameter and thermal Grashof number results in increase in the velocity and decrease temperature and concentration respectively. An increase in the thermophoresis, thermal conductivity leads to increase in temperature and concentration distributions in the system.

Keywords: MHD, exponentially stretching sheet, nanofluid, nonuniform heat generation/absorption, radiation.

Date of Submission: 08-01-2022

Date of Acceptance: 23-01-2022

I. Introduction

The study of nanofluid flow over a sheet that is exponentially stretching is continuously making waves in the field of science and technology due to its important usefulness in the industries, engineers and experts in the technological advancement. Meanwhile, the use of these fluid under consideration in reducing heat in the industries can help in energy saving, lowering of the high rate of emissions and elongating the life span of such systems.

It's vital to add that the various applications of this study are enormous and well appreciated in the metallurgical industries as long as modern technological development, improvement and processes are concerned, production of papers, glass fiber production (blowing and spinning), spinning of steel, aluminum alloy and metals as well as metals and plastic Extrusion, etc. However, continuous strips or filaments cooling occurs when such strips are drawn through a fluid that is at rest (quiescent fluid). Meanwhile, as these strips are drawn, often they're stretched. In addition, the rate at which the strips cool and are stretched is being controlled by passing them across such a fluid just as the durability and how strong the product appears is a function of the cooling rate of the strip as well as the process of stretching.

Nanofluid is said to be a composite of solid-liquid mixture of nanoparticles of sizes 1-100nm. It consists of a liquid called base fluid such as ethyl glycol, water, oil etc., and solid particles known as nanoparticles. The use of nanofluid is essential due to their high thermal conductivity properties. This study has applications in the areas of blowing and spinning of glass, paper production, drawing of wires and sheets of fiber, steel, metals and aluminum alloy spinning, and drawing of plastic films. During the processes, the transfer of heat between the sheet and medium of the fluid takes place and as a result of this, the material needs to be stretched. Meanwhile, the cooling and stretching of the sheet is very important, hence the quality of the product is dependent on the rate at which the cooling and stretching takes place.

Eastman *et al.* (2001) and Choi and Eastman *et al.* (2001) opined that a little quantity (< 1% volume fraction) of copper *Cu* smaller particles embedded in ethylene glycol raises an underlying very low heat conductivity of the liquid. the mechanical properties of the sheet obtained is dependent on the thermal conductivity assumed to change linearly with temperature (Chaudhary and Jain, 2006). Choi (1995), was the first to introduce a new and better fluid type known as nanofluid while studying about fresh facts on how to reduce heat from devices and technology behind it. However, in the work of Eastman *et al* (1997), there is a rise in the heat conductivity of water as smaller particles of copper (II) oxide (*CuO*) of 5% were added to the water.

Waini *et al.* (2020), analyzed the mixed convection flows of hybrid nanofluid over an exponentially stretched medium. They observed that the solid nanoparticles lead to a decrease in the profiles of the flow and enhanced the thermal distribution. Patil *et al.* (2019), discussed the influence of roughness upon mixed convection nanoparticle flow over an exponentially stretched surface. They observed that the rate of flow of heat energy (thermal energy) of the wall is considerably checked by the addition of nanoparticles. Nadeem *et al.* (2020), studied the influence of slip effects over nanoparticle flow over a stretching sheet. They reported that with augmentation of stretching parameter, the microorganism and Nusselt numbers increased while the skin friction decreased. Radiation effects in heat and mass transfer are important in fluid flow. Studies considering the effects of radiation in different flow configurations have been carried out, (Bunonyo *et al.* (2018), Omamoke *et al.* (2020)). The impact of thermal radiations on Maxwell nanoparticle flow upon a stretching cylinder by using semi-analytical method was analyzed by Islam *et al.* (2020). They opined that as a result of the enhancement in Maxwell parameter, the stress relaxation phenomenon was augmented thereby leading to a decrease in the fluid flow.

Khan *et al.* (2020), investigated the MHD Maxwell fluid flowing on the stretched surface. In their investigation, the heat and mass transmission were examined by using the impacts of variations in thermal conductivity and the Cattaneo-Christove effects. They found out that with an augmentation in Deborah factor, more resistance was offered to the fluid flow particles that have caused a decrease in the flow and concentration of fluid and also increased the characteristics of the heat energy (thermal energy). In the same vein, Hamid *et al.* (2015), adopted Buongiorno's model for the investigation of the stagnation-point flow of nanofluid over a stretching/shrinking sheet with suction and injection. According to their results, the local Nusselt number decreases with increasing Brownian motion and thermophoresis parameters just as the Lewis number is independent of the type of sheet (stretching or shrinking) and value of suction and blowing. They opined that the reason behind the thickening of the thermal boundary layer and consequently reduction of Nusselt number might not be unconnected to the increase in the collision between the particles in the whole system (the increase in kinetic energy of the nanoparticles). This is evident as increase in the Brownian motion and thermophoresis parameters leads to an increase in the kinetic energy of the particles. Therefore, Fatunmbi *et al.* (2020), analyzed micropolar MHD fluid flow past a porous medium using slip conditions. They noted that augmentation in stretching parameter exhibits an adverse effect on both the flow and heat energy profiles respectively. Loganathan and Rajan (2020), investigated an entropy approach of Williamson nanofluid flow with joule heating and zero nanoparticle mass flux. They found out that the velocity profile decreases while the temperature profile is enhanced as the magnetic number increases.

Moreover, the mechanical properties of the sheet obtained is dependent on the heat conduction expected to alteration in a straight line with coldness or hotness (Chaudhary and Jain, 2006).

Chamkha *et al.* (2016), carried out a study on unsteady magnetohydrodynamic natural convection drift over an exponentially enhanced upright sheet in the presence of mass transmission, chemical and heat radiation applying Laplace transform method. They considered gray gas fluid, engrossing/releasing radiation without smattering intermediate. Their result showed the velocity enhances as the acceleration coefficient a or the Soret factor S_o enhances.

However, a fascinating result of MHD fluid flows and heat transfer by employing different flow conditions were presented by Khan *et al.* (2021, 2020). They observed augmented values of the magnetic parameter leads to enhancement in transmission of heat and a decrease in the pattern in which the fluid flows. Sheremet *et al.* (2016), surveyed the free convection in a right-angle trapezoidal jam-packed by spongy intermediate and nanofluid by numerical method. Effect of some parameters were considered and they opined that Nusselt and Sherwood numbers enhances as a result of increasing $\frac{g\beta(T_w - T_\infty)L^3}{v\alpha}$. Rashad *et al.* (2013), examined free and forced convective non-Newtonian flow past an upright material externally immersed in a permeable intermediate containing nanofluid. They reported from their findings that a rise in the local heat transfer coefficient is as a result of rises in Gr, Nt, N, θ_s, L . Sheremet *et al.* (2015), investigated an unsteady free convection analysis in a porous cavity with wavy wall saturated by a nanofluid. They concluded that by adjusting the surface geometry parameters of the wavy wall, the average Nusselt and Sherwood numbers could be optimized.

From the studies examined above, none of them investigated the influence of exponential stretching sheet with non-uniform heat generation/absorption and radiation on hydromagnetic nanofluid flow, hence, this analysis.

II. Mathematical Formulation

We considered a steady hydromagnetic two-dimensional boundary layer flow of a nanofluid over an exponentially stretching sheet with the consideration of the thermal radiation and conductivity, heat generation/absorption and stretching sheet parameters. The effects of mass Grashof, thermal conductivity, Brownian motion, thermal radiation and stretching sheet parameters on the flow has been put into consideration

on the flow model. We assume that the nanoparticles are dispersed homogeneously in the base fluid. The Cartesian coordinates (x, y) is used with $y - axis$ as the vertical plate and $x - axis$ along the sheet.

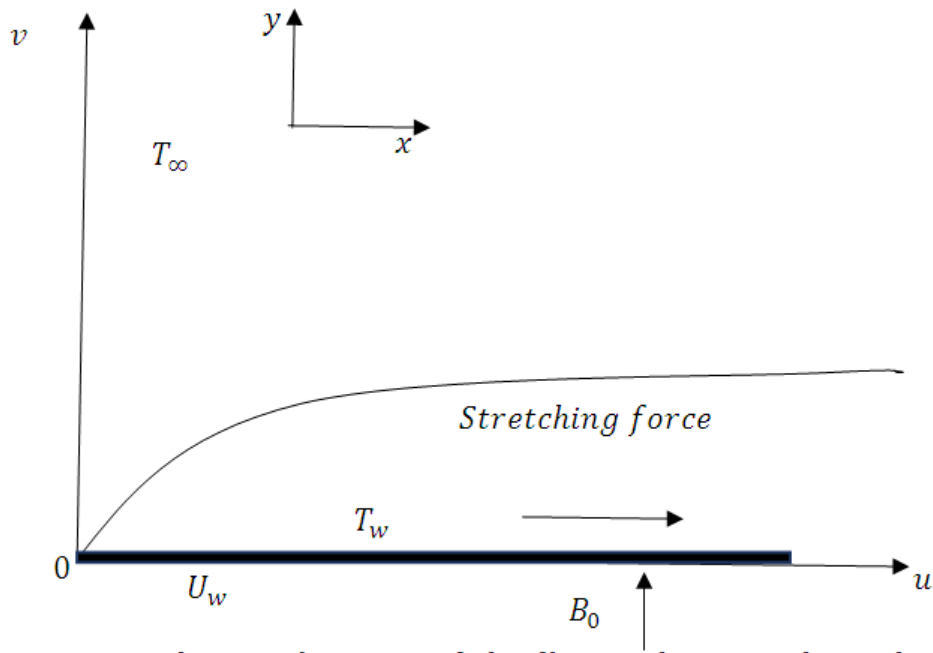


Figure 1. Schematic diagram of the flow with a stretching sheet

The corresponding velocity components are v , for y -axis and u , for $x - axis$. The temperature, T and nanoparticles volume fraction C at the boundary ($y = 0$) are T_w and C_w respectively while far from the plate the temperature and nanoparticles fraction are T_∞ and C_∞ respectively. We applied a uniform magnetic field of strength B_0 along the x -axis and assume that the magnetic Reynolds number is small, hence the induced magnetic field is negligible and consequently considered only the applied magnetic field. With the above considerations, the boundary layer governing equations can be expressed as follows:

$$\frac{\partial u}{\partial x} + \frac{\partial v}{\partial y} = 0$$

(1)

$$\rho_f \left(u \frac{\partial u}{\partial x} + v \frac{\partial u}{\partial y} \right) = \mu \frac{\partial^2 u}{\partial y^2} - \sigma B_0^2 u + (1 - C_\infty) \rho_\infty \beta g (T - T_\infty) + (\rho_p - \rho_{f_\infty}) g (C - C_\infty) \quad (2)$$

$$u \frac{\partial T}{\partial x} + v \frac{\partial T}{\partial y} = \frac{k}{(\rho c)_f} \frac{\partial^2 T}{\partial y^2} + \frac{(\rho c)_p}{(\rho c)_f} \left[D_B (C - C_\infty) (T - T_\infty) + \frac{D_T}{T_\infty} (T - T_\infty) \right] - \frac{1}{(\rho c)_f} \frac{\partial q_r}{\partial y} + \frac{1}{(\rho c)_f} q''' \quad (3)$$

$$u \frac{\partial C}{\partial x} + v \frac{\partial C}{\partial y} = D_B \frac{\partial^2 C}{\partial y^2} + \frac{D_T}{T_\infty} (T - T_\infty) - \frac{1}{(\rho c)_f} q''' \quad (4)$$

With the following boundary conditions

$$\left. \begin{aligned} u = U_w(x) = a e^{\frac{x}{L}}, \quad v = -v_w, \quad T = T_w, \quad C = C_\infty \quad \text{at } y = 0 \\ u \rightarrow U_\infty(x) = b e^{\frac{x}{L}}, \quad T \rightarrow T_\infty, \quad C \rightarrow C_\infty \quad \text{as } y \rightarrow \infty \end{aligned} \right\} \quad (5)$$

where, ρ_p is the nanoparticle density, ρ_f is the base fluid density, β is volumetric thermal expansion coefficient of the base fluid, σ is electrical conductivity parameter, g is the acceleration due to gravity, k is thermal conductivity, μ is viscosity of the fluid, D_T is thermophoresis diffusion parameter, k_r is the chemical reaction parameter, q_r is the radiative heat flux and q''' is the temperature dependent non-uniform heat source/sink defined in Hakeem et al (2017) as:

$$q''' = \frac{k R a_x^{\frac{1}{2}}}{2 x^2} [A (T_w - T_\infty) S'(\eta) + B (T - T_\infty)] \quad (6)$$

The similarity variables are defined as follows:

$$\eta = \sqrt{\frac{a}{2 v L}} e^{\frac{x}{2 L}} y, \quad \psi = \sqrt{2 v L a} e^{\frac{x}{2 L}} S(\eta), \quad \theta(\eta) = \frac{T - T_\infty}{T_w - T_\infty}, \quad W(\eta) = \frac{C - C_\infty}{C_w - C_\infty} \quad (7)$$

$$u = \frac{\partial \psi}{\partial y}, \quad v = -\frac{\partial \psi}{\partial x}$$

III. Method of solution

For us to obtain the solution, we shall use the variables in equation (7) to transform the equations in order to have:

$$S''''(\eta) + S(\eta)S''(\eta) - MS'(\eta) + Gr\theta(\eta) + Bm\phi(\eta) = 0 \tag{8}$$

$$\left(1 + \frac{4}{3}R\right)\theta''(\eta) + PrS(\eta)\theta'(\eta) + N_b\theta(\eta)\phi(\eta) + N_t\theta(\eta) + AKS'(\eta) + BK\theta(\eta) = 0 \tag{9}$$

$$\phi''(\eta) + ScS(\eta)\phi'(\eta) + \frac{N_t}{N_b}\theta(\eta) - AKS'(\eta) + BK\phi(\eta) = 0 \tag{10}$$

Therefore, the transformed boundary conditions are as follows:

$$\left. \begin{aligned} S(0) = s_0, \quad S'(0) = 1, \quad \theta(0) = 1, \quad \phi(0) = 1 \quad \text{at } \eta = 0 \\ S'(\infty) = \lambda, \quad \theta(\infty) \rightarrow 0, \quad \phi(\infty) \rightarrow 0 \quad \text{as } \eta \rightarrow \infty \end{aligned} \right\} \tag{11}$$

where,

$$M = \frac{2\sigma B_0^2 L}{(1-c_\infty)\rho_f U_w}, \text{ is the modified magnetic parameter, } Gr = \frac{2L\beta g(T_w - T_\infty)}{(1-c_\infty)U_w^2}, \text{ is the thermal Grashoff number,}$$

$$Bm = \frac{2L(\rho_p - \rho_f \infty)g(c_w - c_\infty)}{(1-c_\infty)\rho_f U_w^2}, \text{ is the solutal Grashof parameter, } R = \frac{4T_\infty^3 \sigma_0^*}{k^* k} \Rightarrow \text{radiation factor, } K = \frac{\tau L}{U_w R a_x^{\frac{1}{2}}} \Rightarrow$$

conductivity parameter, $Pr = \frac{\nu}{\alpha} \Rightarrow$ Prandtl number,

$$N_b = \frac{2L\alpha_D B(c_w - c_\infty)}{U_w} \Rightarrow \text{Brownian diffusion effect, } N_t = \frac{2\mu L D_T(T_w - T_\infty)}{\nu T_\infty} \Rightarrow \text{thermophoresis parameter, } = \frac{\nu}{D_B},$$

Schmidt number, and the primes represent differentiation with respect to η , $s_0 = \frac{\nu_w}{\sqrt{\frac{av}{2L}}}$ is the suction parameter.

In order to solve equations (8)-(10) with boundary equation (11), we follow Bestman (1990), thus,

$$\eta = \delta s_0, \quad s(\eta) = s_0 S(\eta), \quad \theta(\eta) = \theta(\eta), \quad W(\eta) = \phi(\eta), \quad \xi = \frac{1}{s_0^2} \tag{12}$$

and the resulting equations are:

$$S''''(\eta) + S(\eta)S''(\eta) - \xi MS'(\eta) + \xi^2 Gr\theta(\eta) + \xi^2 Bm\phi(\eta) = 0 \tag{13}$$

$$\theta''(\eta) \left(1 + \frac{4}{3}R\right) + PrS(\eta)\theta'(\eta) + \xi N_b\theta(\eta)\phi(\eta) + \xi N_t\theta(\eta) + AKS'(\eta) + \xi BK\theta(\eta) \tag{14}$$

$$\phi''(\eta) + ScS(\eta)\phi'(\eta) + \xi \frac{N_t}{N_b}\theta(\eta) - AKS'(\eta) + \xi BK\phi(\eta) = 0 \tag{15}$$

subject to:

$$S(0) = 1, S'(0) = \xi, S'(\infty) = \xi\lambda, \theta(0) = 1, \theta(\infty) = 0, \phi(0) = 1, \phi(\infty) = 0 \tag{16}$$

For $\xi \ll 1$ (large suction), we adopt asymptotic series technique, Bestman (1990):

$$S(\eta) = 1 + \xi S_1(\eta) + \xi^2 S_2(\eta) + \dots \tag{17}$$

$$\theta(\eta) = \theta_0(\eta) + \xi \theta_1(\eta) + \dots \tag{18}$$

$$\phi(\eta) = \phi_0(\eta) + \xi \phi_1(\eta) + \dots \tag{19}$$

Using equations (17) – (19) on equations (13) – (6) and after differentiations and simplification we obtain the series of approximations as:

$$\left(1 + \frac{4}{3}R\right)\theta_0''(\eta) + Pr\theta_0'(\eta) = 0 \tag{20}$$

$$\phi_0''(\eta) + Sc\phi_0'(\eta) = 0 \tag{21}$$

$$S_1''''(\eta) + S_1''(\eta) = 0 \tag{22}$$

$$\left(1 + \frac{4}{3}R\right)\theta_1''(\eta) + Pr\theta_1'(\eta) + PrS_1(\eta)\theta_0'(\eta) + N_b\theta_0(\eta)\phi_0(\eta) + N_t\theta_0(\eta) + AKS_1'(\eta) + BK\theta_0(\eta) = 0 \tag{23}$$

$$\phi_1''(\eta) + ScS_1(\eta)\phi_0'(\eta) + Sc\phi_1'(\eta) + \frac{N_t}{N_b}\theta_0(\eta) - AKS_1'(\eta) + BK\theta_0(\eta) = 0 \tag{24}$$

$$S_2''''(\eta) + S_2''(\eta) + S_1(\eta)S_1'(\eta) - MS_1'(\eta) + Gr\theta_0(\eta) + Bm\phi_0(\eta) = 0 \tag{25}$$

Subject to

$$\left. \begin{aligned} \theta_0(0) = 1, \theta_0(\infty) = 0; \phi_0(0) = 1, \phi_0(\infty) = 0; S_1(0) = 0, S_1'(\infty) = \lambda \\ \theta_1(0) = 0, \theta_1(\infty) = 0; \phi_1(0) = 0, \phi_1(\infty) = 0; S_2(0) = 0, S_2'(0) = 0, S_2'(\infty) = 0 \end{aligned} \right\} \tag{26}$$

Solving equations (20) – (25) subject to equation (26) gives the results below:

$$S'(\eta) = \lambda - \lambda e^{-\eta} + e^{-\eta} + \frac{(\lambda)^2}{2}(\eta)^2 e^{-\eta} - (\lambda)^2 e^{-\eta} - \frac{\lambda}{2}(\eta)^2 e^{-\eta} + \lambda \eta e^{-\eta} - \eta e^{-\eta} - \frac{(\lambda)^2}{2} e^{-2\eta} + \frac{3\lambda}{4} e^{-2\eta} - \frac{1}{2} e^{-2\eta} + M\lambda\eta - M\lambda + M\lambda\eta e^{-\eta} - M\lambda e^{-\eta} - M\eta e^{-\eta} + M\eta e^{-\eta} - \frac{Gr}{q(q-1)} e^{-q\eta} - \frac{Bm}{Sc(Sc+1)} e^{-Sc\eta} + M\lambda - M\lambda\eta + \left(\frac{3\lambda}{2} - 2\lambda + \frac{1}{2} + 2M\lambda - M + \frac{Gr}{q(q-1)} + \frac{Bm}{Sc(Sc-1)} - M\lambda + M\lambda\eta\right) e^{-\eta} \quad (27)$$

$$\theta(\eta) = e^{-q\eta} + \left(-\frac{q\lambda}{2}\eta^2 e^{-q\eta} - \lambda\eta e^{-q\eta} + q\lambda\eta e^{-q\eta} - q\eta e^{-q\eta} + \frac{q^2\lambda}{1+q} e^{-(1+q)\eta} - \frac{q^2}{1+q} e^{-(1+q)\eta} - \frac{3N_b}{Sc(3+4R)((q+Sc))} e^{-(Sc+q)\eta} + \frac{3N_t}{q(3+4R)} \eta e^{-q\eta} - \frac{3AK\lambda}{q(3+4R)} \eta + \frac{3AK\lambda}{q^2(3+4R)} + \frac{3AK\lambda}{(3+4R)((1-q))} e^{-\eta} - \frac{3AK}{(3+4R)((1-q))} e^{-\eta} + \frac{3BK}{q(3+4R)} \eta e^{-q\eta} + \frac{3AK\lambda}{q(3+4R)} \eta - \frac{3AK\lambda}{q^2(3+4R)} - \frac{q^2\lambda}{1+q} + \frac{q^2}{1+q} + \frac{3Nb}{Sc(3+4R)((q+Sc))} - \frac{3AK\lambda}{(3+4R)((1-q))} + \frac{3AK}{(3+4R)((1-q))} - \frac{3AK\lambda}{q(3+4R)} \eta\right) \quad (28)$$

$$\phi(\eta) = e^{-Sc\eta} + \left(-\frac{Sc\lambda}{2}\eta^2 e^{-Sc\eta} - \lambda\eta e^{-Sc\eta} + Sc\lambda\eta e^{-Sc\eta} - Sc\eta e^{-Sc\eta} + \frac{(Sc)^2\lambda}{1+Sc} e^{-(1+Sc)\eta} - \frac{(Sc)^2}{1+Sc} e^{-(1+Sc)\eta} - \lambda\eta e^{-Sc\eta} - \frac{Sc\lambda}{1+Sc} e^{-(1+Sc)\eta} - \frac{Sc}{1+Sc} e^{-(1+Sc)\eta} - \frac{N_t}{qNb(q-Sc)\eta} e^{-q\eta} + \frac{AK\lambda}{Sc} \eta - \frac{AK\lambda}{(Sc)^2} - \frac{AK\lambda}{1-Sc} e^{-\eta} - \frac{AK}{1-Sc} e^{-\eta} + \frac{BK}{sc} \eta e^{-Sc\eta} + \frac{AK\lambda}{(Sc)^2} - \frac{AK\lambda}{Sc} \eta - \frac{(Sc)^2\lambda}{1+Sc} e^{-Sc\eta} + \frac{(Sc)^2}{1+Sc} e^{-Sc\eta} + \frac{Sc\lambda}{1+Sc} e^{-Sc\eta} + \frac{Sc}{1+Sc} e^{-Sc\eta} + \frac{N_t}{qNb(q-Sc)\eta} e^{-Sc\eta} + \frac{AK\lambda}{(Sc)^2} e^{-Sc\eta} + \frac{AK}{1-Sc} e^{-Sc\eta} + \frac{AK\lambda}{Sc} \eta e^{-Sc\eta}\right) \quad (29)$$

IV. Results and Discussion

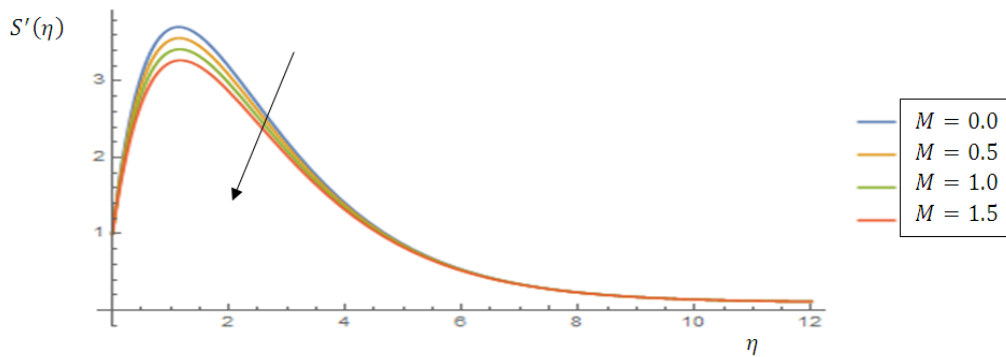


Figure 1: Effect of the Magnetic parameter M , on velocity with $\lambda = 0.1, Gr = 5.0, Pr = 0.71, Br = 0.1, R = 0.1, Sc = 5.0$

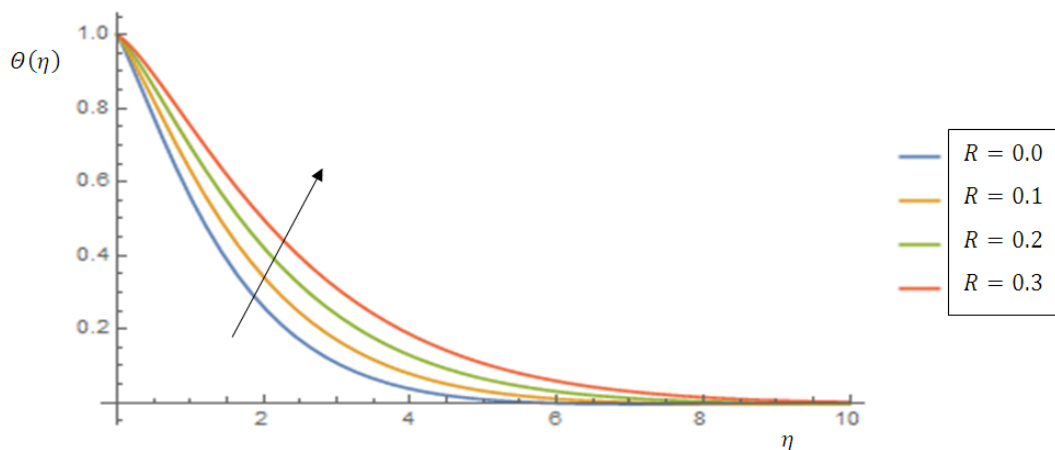


Figure 2: Effect of Radiation R , on Temperature with $A = B = K = 0.1, Nt = Nb = 0.5, Pr = 0.71, Sc = 5.0, \lambda = 0.1$

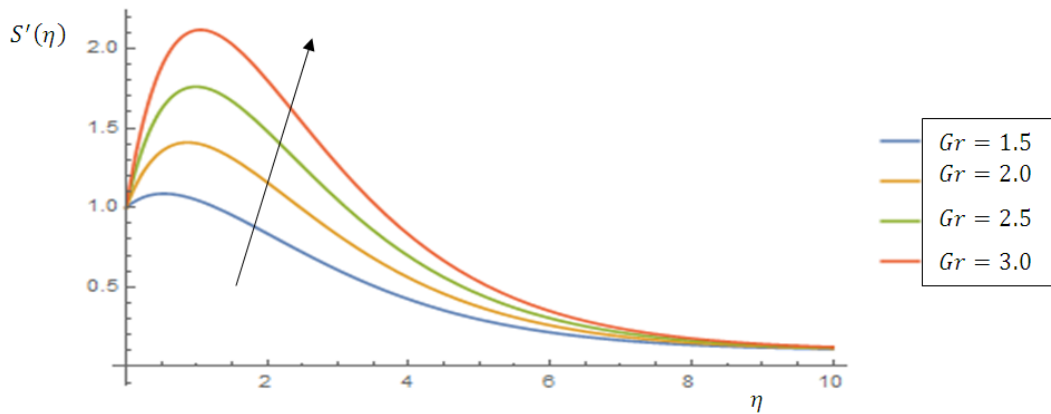


Figure 3: Effect of the Grashoff parameter Gr , on velocity with $\lambda = 0.1, M = 0.5, Pr = 0.71, Br = 0.1, R = 0.1, Sc = 5.0$

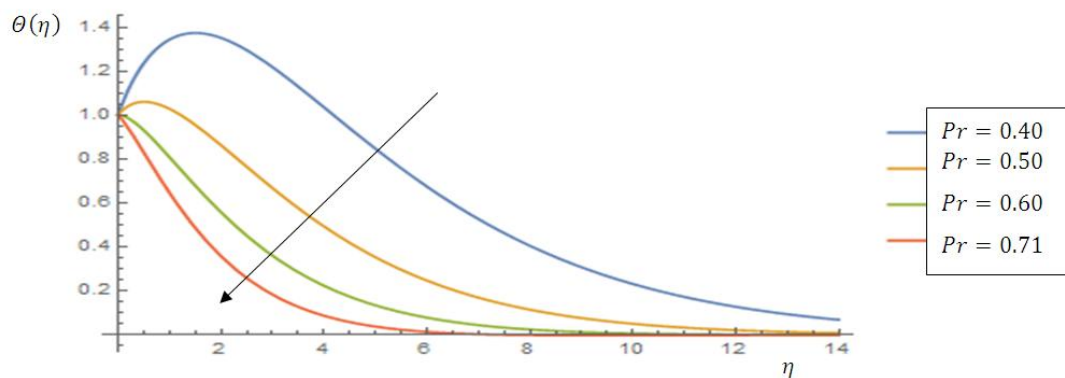


Figure 4: Effect of Prandtl number Pr , on Temperature with $A = B = K = 0.1, Nt = Nb = 0.5, R = 0.1, Sc = 5.0, \lambda = 0.1$

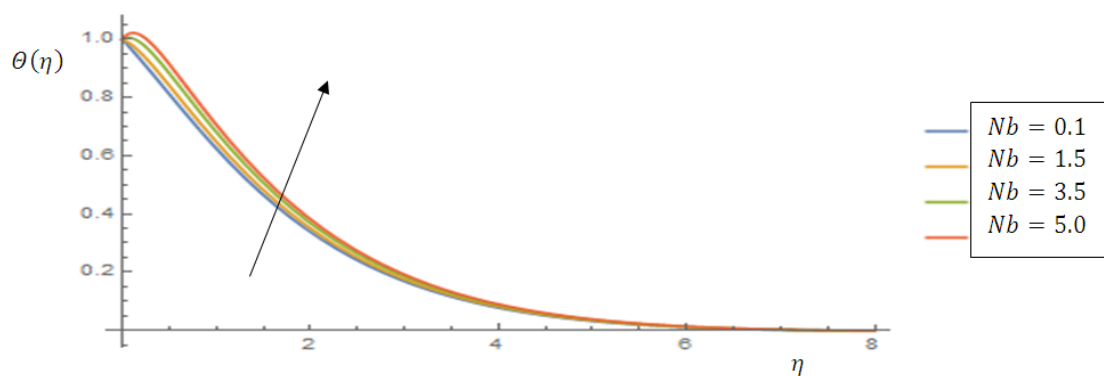


Figure 5: Effect of Brownian motion parameter Nb , on Temperature with $A = B = K = 0.1, Nt = 0.5, Pr = 0.71, Sc = 5.0, \lambda = 0.1, R = 0.1$

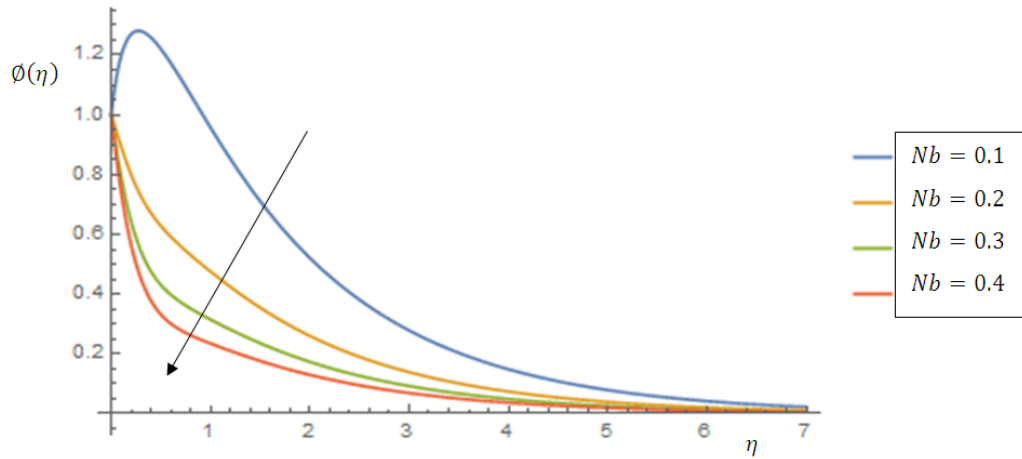


Figure 6: Effect of Brownian motion parameter Nb , on Concentration with $Pr = 0.71, Nt = 0.5, Sc = 5.0, K = A = B = \lambda = R = 0.1$

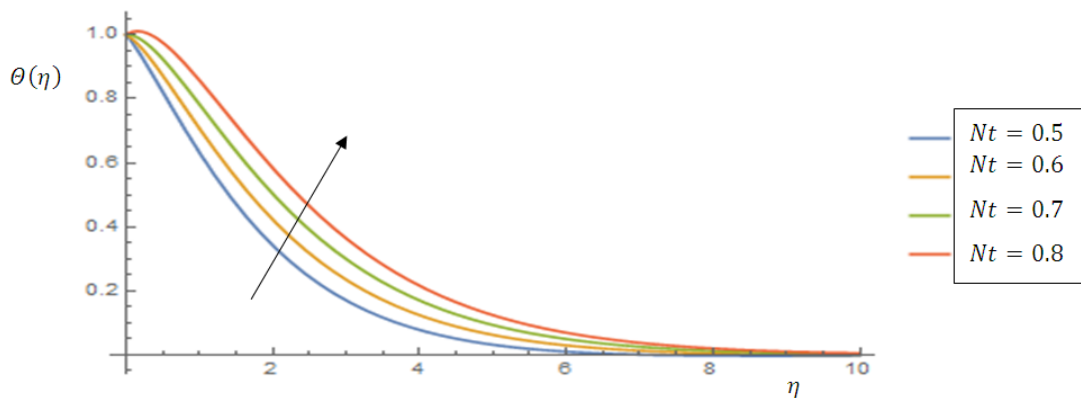


Figure 7: Effect of Thermophoresis parameter Nt , on Temperature with $A = B = K = 0.1, Nb = 0.5, Pr = 0.71, Sc = 5.0, \lambda = 0.1, R = 0.1$

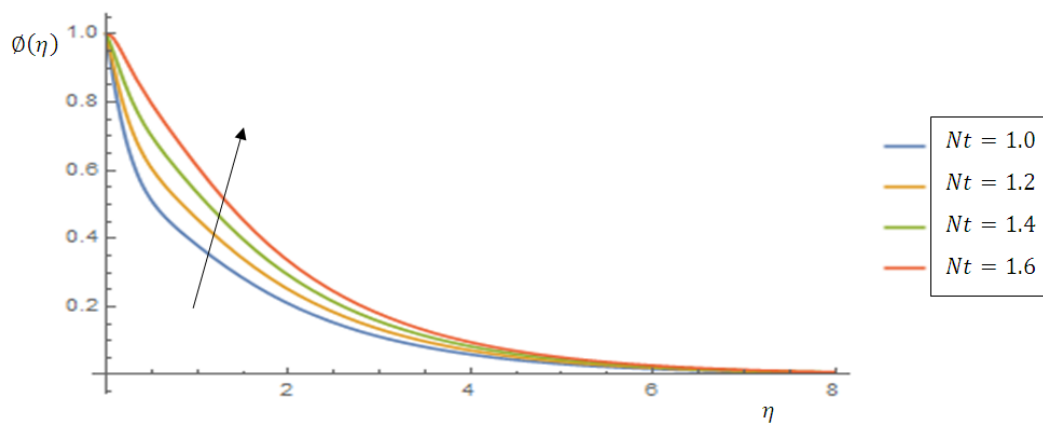


Figure 8: Effect of Thermophoresis parameter Nt , on Concentration with $Pr = 0.71, Nb = 0.5, Sc = 5.0, K = A = B = \lambda = R = 0.1$

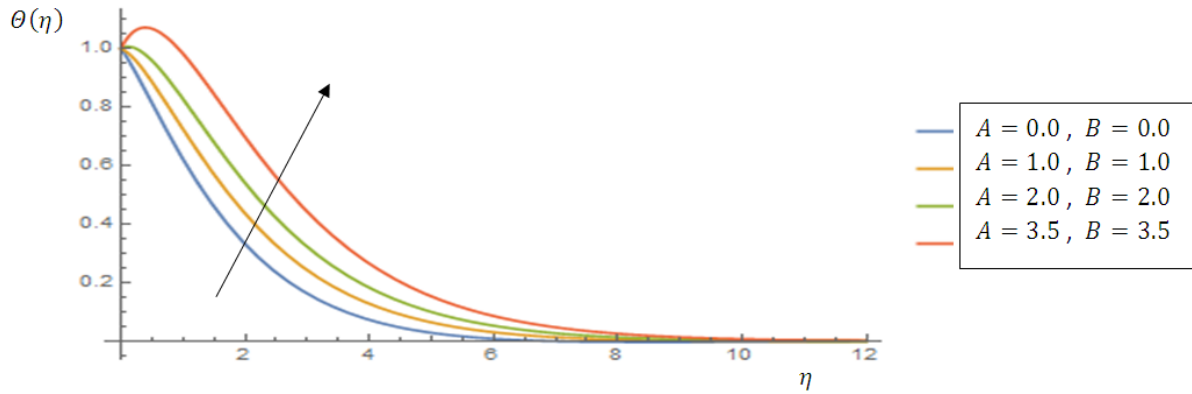


Figure 9: Effect of Heat generation parameters $A > 0, B > 0$, on Temperature with $K = 0.1, Nb = Nt = 0.5, Pr = 0.71, Sc = 5.0, \lambda = 0.1, R = 0.1$

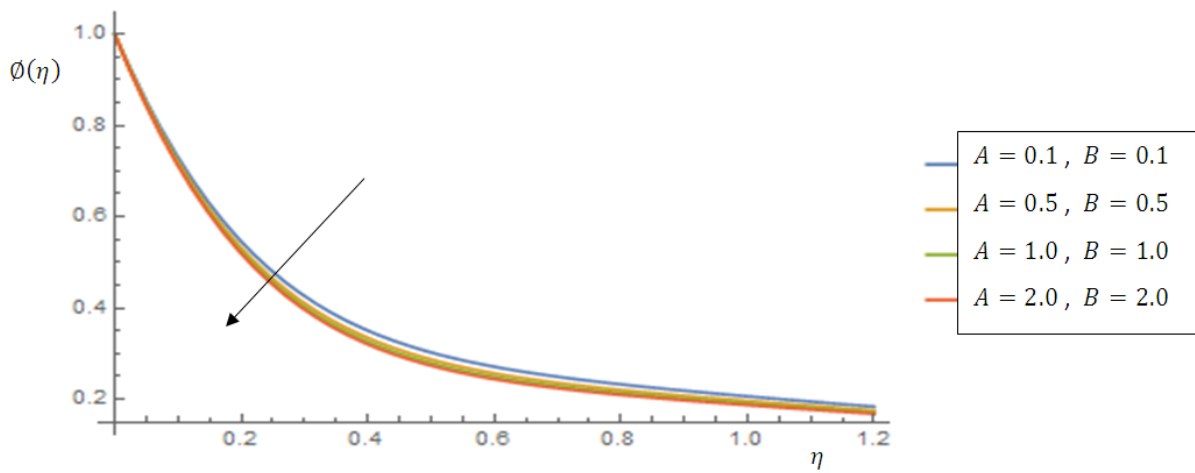


Figure 10: Effect of Heat generation parameters $A > 0, B > 0$, on Concentration with $Nb = Nt = 0.5, Sc = 5.0, K = \lambda = R = 0.1, Pr = 0.71$

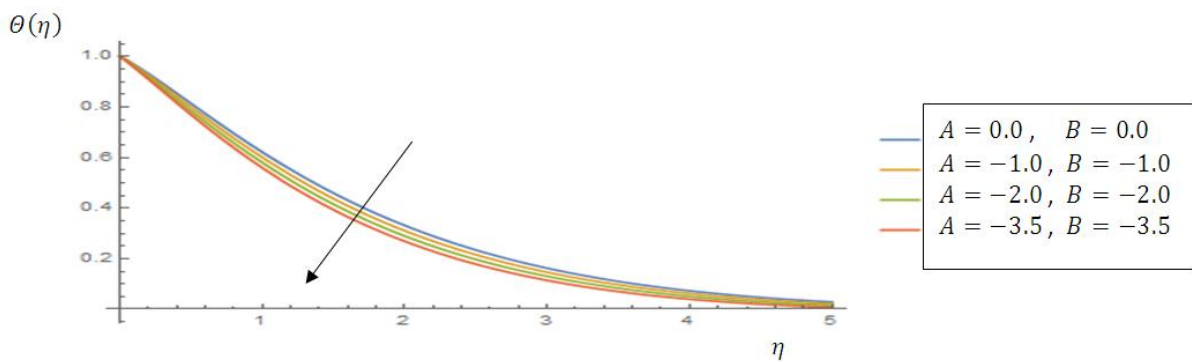


Figure 11: Effect of Heat absorption parameters $A < 0, B < 0$, on Temperature with $K = 0.1, Nb = Nt = 0.5, Pr = 0.71, Sc = 5.0, \lambda = 0.1, R = 0.1$

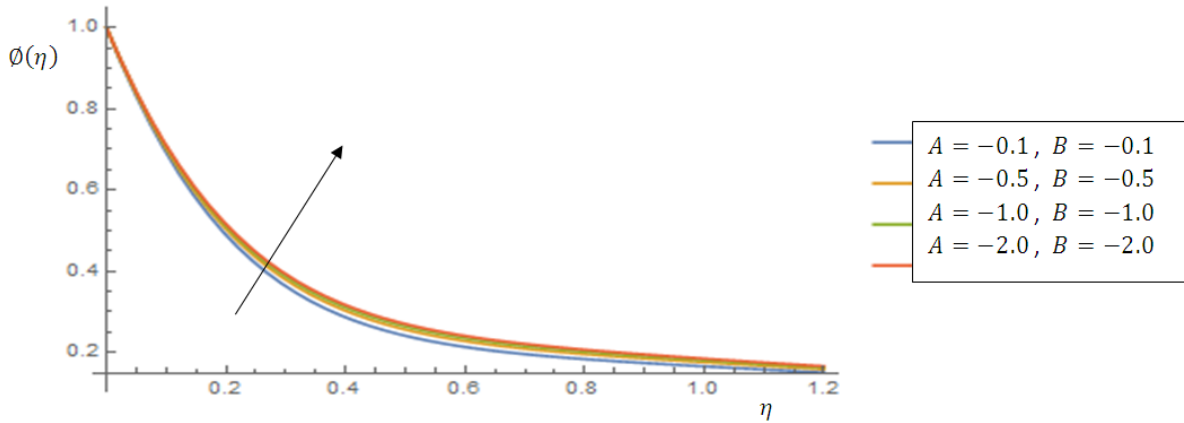


Figure 12: Effect of Heat absorption parameters $A < 0, B < 0$, on Concentration with $Nb = Nt = 0.5, Sc = 5.0, K = \lambda = R = 0.1, Pr = 0.71$

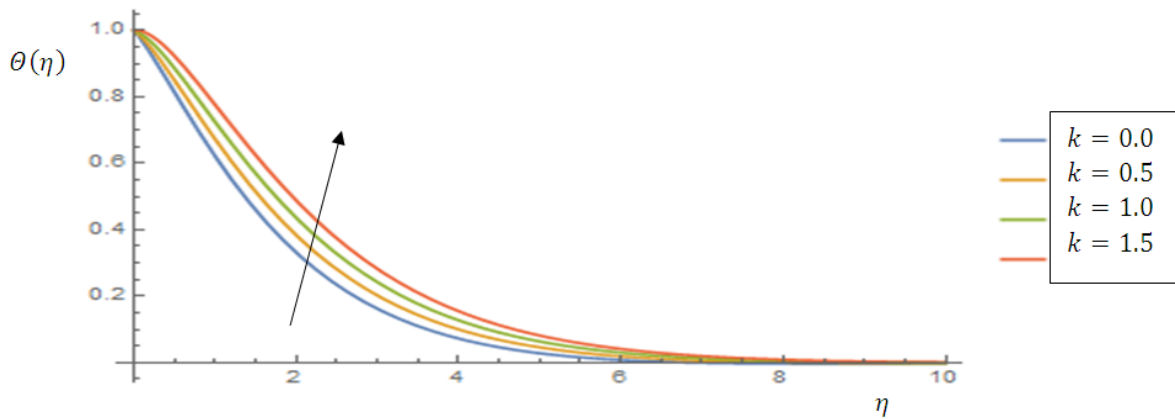


Figure 13: Effect of thermal conductivity parameter k , on Temperature with $A = B = 0.1, Nt = Nb = 0.5, Pr = 0.71, Sc = 5.0, \lambda = 0.1, R = 0.1$

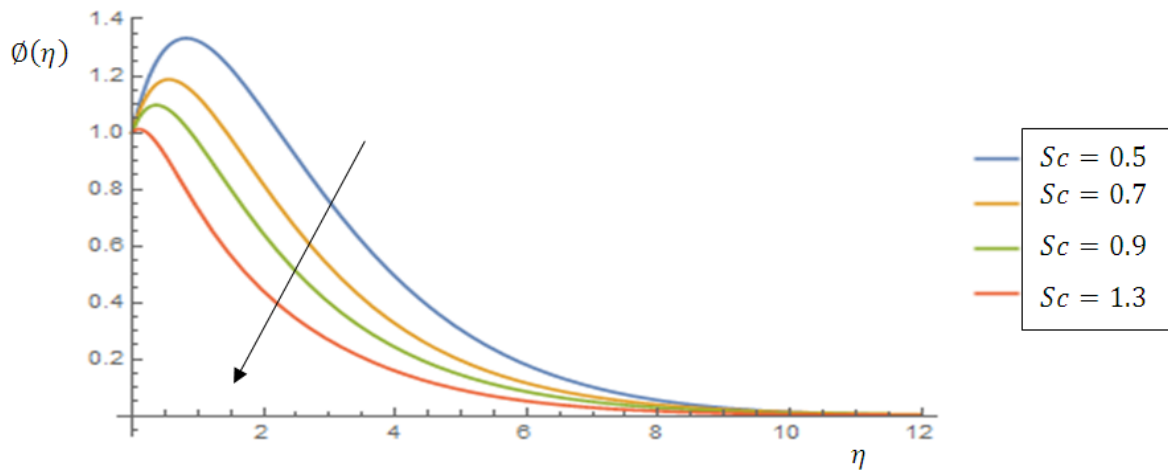


Figure 14: Effect of Schmidt number Sc , on Concentration with $R = 0.1, Nb = Nt = 0.5, Pr = 0.71, K = A = B = \lambda = 0.1$

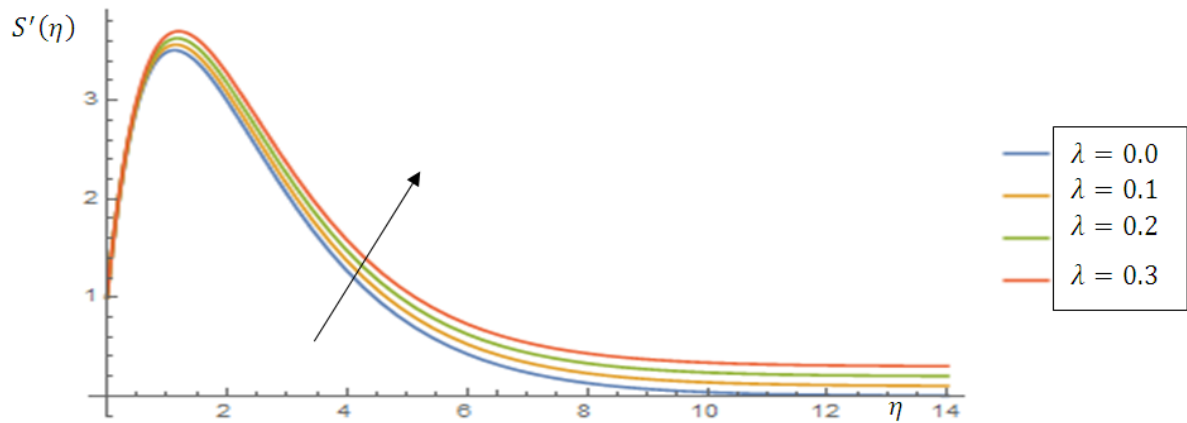


Figure 15: Effect of the stretching sheet parameter λ , on velocity with $M = 0.5, Gr = 5.0, Pr = 0.71, Gm = 0.1, R = 0.1, Sc = 5.0$

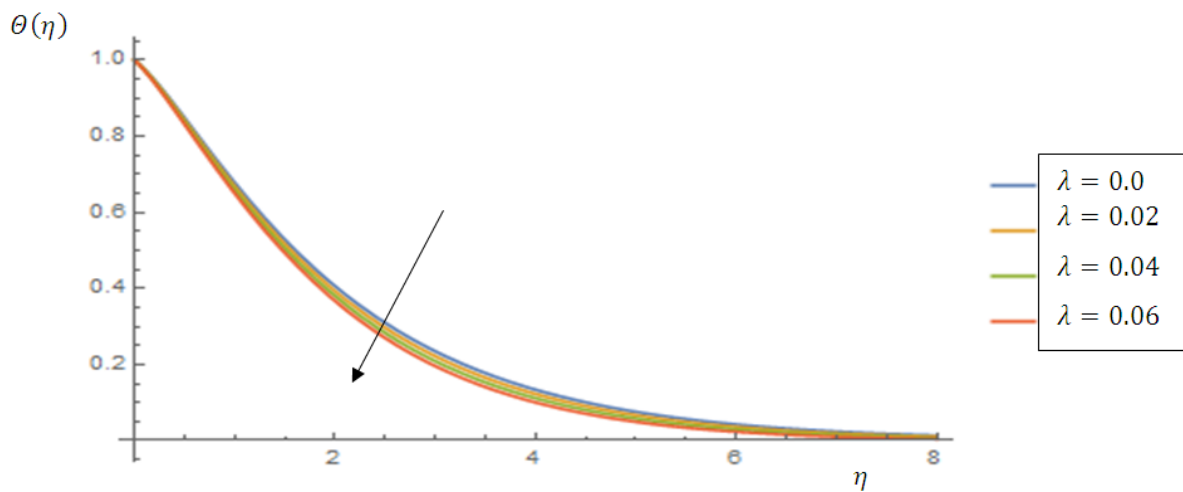


Figure 16: Effect of the stretching sheet parameter λ , on Temperature with $A = B = K = 0.1, Nt = Nb = 0.5, R = 0.1, Pr = 0.71, Sc = 5.0$

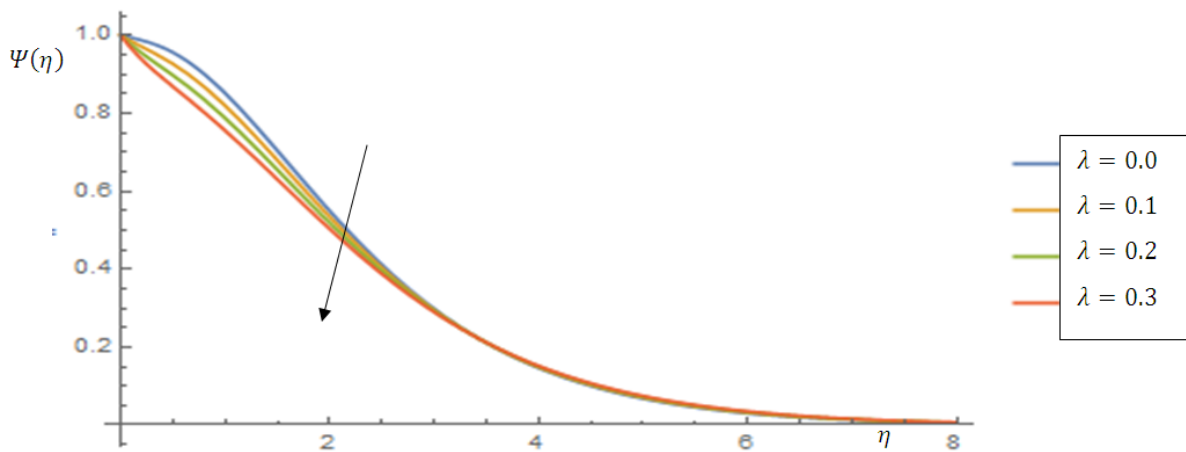


Figure 17: Effect of the stretching sheet parameter λ , on Concentration with $R = Nt = Nb = \gamma = 0.1, Gr = 5.0, Pr = 1.1$.

V. Discussion of Results

The analysis of the fluid parameters involved in this study are presented as follows:

The impact of variations of values of the magnetic parameter M , on fluid motion is showcase through figure 1. For a given good conductor of fluid, the application of magnetic field in a direction normal to it produces a certain power which acts in an opposite route to the fluid flow. This force which resists or drags the velocity of the fluid flow backward is termed the Lorentz force. Thus, as this parameter M increase, the velocity of the fluid flow decreases.

The influence of the variations in radiation parameter R , on the nanofluid temperature are presented in figures 2. However, the increase in radiation parameter R , generates more thermal energy (heat) to the nanofluid and this increases the thermal boundary layer and temperature as shown in figure 2.

The influence of the thermal Grashof number Gr on velocity is depicted in figure 3. This parameter relates the impact of the thermal buoyancy forces to viscous force within the boundary layer region and an increase in the thermal buoyancy force brings about a growth in the nanofluid velocity. However, as values of Gr intensifies, there is a sharp increase in the velocity near the sheet which gradually decreases.

The influence of the Prandtl number Pr , on the nanofluid temperature is shown in figures 4 accordingly. As Pr increases, the temperature of the nanofluid reduces. This is true because physically, a fluid with large Prandtl number is associated with low thermal diffusivity causing the thermal energy (heat) penetration to be low. Hence, a reduction in the thermal boundary layer thickness sets in.

The stimulus of the Brownian motion parameter Nb on nanofluid temperature and concentration fields are depicted in figures 5 and 6. Increasing the Brownian motion parameter, leads to increase in the heat energy boundary layer and temperature of the nanofluid. This is attributed to the porosity nature of nanofluid within the hydrodynamic and thermal boundary layers. In figure 6, as Nb increases, the concentration decreases. This is because increasing the Brownian motion is associated with more unpredictable motion and haphazard motion as well as the striking of nanoparticles.

The evolution of the effect of thermophoresis parameter Nt , on the nanofluid temperature and concentration is showcase in figures 7 and 8. As the thermophoresis parameter Nt intensifies, the temperature gradient of the nanofluid rises resulting to enhancement in the thickness of the thermal boundary layer. However, the nanoparticles exhibit several reactions to the variation in the value of the Nt because of the force of the temperature rise. Hence, with the rise in Nt , the movement of the nanoparticles becomes faster and this leads to increase in the energy due to motion, thereby bringing about the thickening of the boundary layer and temperature profile. Similarly, a growth in Nt , leads to a rise in the concentration profile. This is caused as a result of random motion of the nanoparticles due to the thermal kinetic energy they have acquired. Hence, an increase in the concentration sets in as presented in figure 8.

However, the heat generation/source parameters A and B shows an impact on temperature and concentration distributions on nanofluid. An increase in its values ($A > 0, B > 0$) is accompanied with an enhancement in the temperature and reduction in the nanoparticle concentration as captured in figures 9 and 10. With the effect of heat generation, the fluid flow changes because a considerable quantity of thermal energy (heat) is been realized and this leads to an increase in the thermal thickness of the boundary layer, thus leading to a rise in the temperature. Conversely, concentration profile decreases as the heat generation/source parameters increases ($A > 0, B > 0$) as it is obvious in figure 10. Meanwhile, since the dispersion of nanoparticles leads to decrement in the rate of transfer of thermal energy, then it shows that heat energy will be loss thereby resulting to a decrease in the mass boundary layer thickness and causes a decrease in the concentration profile.

In figures 11 and 12, the effect of heat absorption parameters ($A < 0, B < 0$) on temperature and concentration are presented. Since as heat absorption ($A < 0, B < 0$) is accompanied by heat loss, then it implies that the heat energy already gained by the particles will be decreasing gradually (until it is lost completely) leading to a fall in the thickness of the thermal boundary layer and consequently in the temperature of the fluid as depicted in figure 11. On the other hand, heat absorption ($A < 0, B < 0$) enhances the concentration distribution as shown in figure 12. As the heat source gradually decreases, the zigzag motion of the particles slows down while mass thermal boundary layer thickness rises and leads to an increase in the concentration.

Figures 13 indicates the impact of the thermal conductivity parameter k , on dimensionless temperature. Meanwhile, increasing the thermal conductivity parameter k results to an increasing thickness of the thermal boundary layers leading to a rise in the temperature.

The Schmidt number Sc , and its influence on the nanoparticle concentration is presented by the use of figures 14. The number Sc , implies the ratio of momentum diffusivity (kinematic viscosity) to mass diffusivity. Physically, it entails the relative thickness of the hydrodynamic layer and mass transfer boundary layer. Hence, increasing Sc causes a decay in the mass boundary layer thicknesses leading to a decrease in concentration.

The effect of the stretching sheet parameter λ , on velocity, temperature and concentration profiles are represented in figures 15, 16 and 17 respectively. As the values of the stretching sheet parameter increases gradually, the velocity of the fluid flow also increases slowly. As the values of the stretching sheet parameter intensifies, the velocity gradient also increases quickly, moving far away from the free stream region thereby allowing more flow to occur. This is attributed to the fact that the velocity of the stretching sheet is less than free stream velocity. This is shown in figure 15. Meanwhile, the effect of stretching sheet parameter on temperature and concentration are presented in figures 16 and 17. It is observed from the profiles that both the temperature and concentration decrease as the stretching sheet parameter increases. This is as a result of the fact that velocity of the stretching sheet is more than the free stream velocity and more energy (heat) is needed to overcome this and also particles move from the area of greater concentration to the area of lower concentration.

VI. Conclusion

Having successfully carried out the analysis of hydromagnetic nanofluid flow past an exponentially stretching sheet with radiation and nonuniform heat generation/absorption analytically, together with the MATHEMATICA for the solution simulation, we have noted vital observations springing from the significance of parameters of nanofluid flow as it affects the velocity, temperature as well as concentration. Hence, we have made the following conclusions from our study.

1. The velocity increases as thermal radiation, stretching sheet, thermal Grashof, numbers rise.
2. Upsurge in the values of magnetic parameters leads to a decline in fluid velocity.
3. Increasing the stretching sheet, Prandtl number and heat absorption ($A < 0, B < 0$) numbers lower the temperature while the reverse is the case when thermal radiation, Brownian motion and heat generation parameters ($A > 0, B > 0$), rises.
3. The effect of thermophoresis and thermal conductivity factors when they are increased brings about increase in temperature and concentration.
4. In the case of increasing values of Brownian motion and heat generation parameters ($A > 0, B > 0$) the concentration decreases while for heat absorption parameters ($A < 0, B < 0$), it rises.

Nomenclature

(u, v)	the velocity components
μ	viscosity coefficient.
ρ	density of fluid.
σ	electrical conductivity of fluid.
M	Magnetic field parameter.
T	fluid temperature.
k	fluid heat conductivity.
C_p	heat capacity at constant pressure.
q_r	heat flux radiative.
C	Concentration.
τ	the proportion of heat capacities of nanofluid to that of base fluid.
$(\rho C)_p$	nanofluid heat capacities.
$(\rho C)_f$	base fluid heat capacities.
D_B	Coefficient of Brownian motion.
D_T	thermophoretic diffusion coefficients
T_∞	the ambient fluid temperature.
C_∞	the ambient fluid concentration.
Pr	Prandtl number.
Sc	Schmidt number.
Nt	thermophoresis number.
Nb	Brownian motion factor.
λ	Stretching sheet velocity parameter.
R	the thermal radiation factor.
Gr	Thermal Grashof parameter.

Statement Interest

To the best of the authors knowledge, there's an absence of conflict of interest.

References

- [1]. Bestman A. R (1990). The boundary-layer flow past a semi-infinite heated porous plate for two-component plasma. *Astrophysics and Space Science*, 173: 93-100.
- [2]. Bunonyo K. W., Amos E., and Eli I. C. (2018). Unsteady oscillatory couette flow between parallel plates with constant radiative flux. *Asian Research Journal of Mathematics*, 11(2), 1-11
- [3]. Choi, S.U.S., Zhang, Z.G., Yu, W., Lockwood, F.E., and Grulke, E.A. (2001). Anomalous Thermal conductivity enhancement in nano-tube suspensions. *Applied physics letters*, 79, 22522254.
- [4]. Choi, S. U. S. and Eastman, J. A. (1995). Enhancing Thermal Conductivity of Fluids with Nano-particles, Argonne National Lab.
- [5]. Chamkha, A. J., Raju, M. C., Sudhakar, R. T. and Varma, S. V. K. (2016). Unsteady MHD Free Convection Flow Past as Exponentially Accelerated Vertical Plate with Mass Transfer, Chemical and Thermal radiation. *International Journal of Microscale and Nanoscale thermal*. 5(1), 57-75.
- [6]. Chaudhary, R. C. and Jain, P. (2006). Unsteady free Convection boundary layer flow past an impulsively started vertical surface with Newtonian heating, *Rom, Joun, Phys.*, vol.51, Nos. 9-10, pp.911-925.
- [7]. Eastman, J. A., Choi, U. S. U., Thompson, L. J. and Lee, S. (1997). Enhanced thermal conductivity through the development of nano-fluids. volume 457 of *Materials Research society Symposium – Proceedings*, 311. Materials Research Society, Pittsburg, PA, USA, Boston, MA, USA.
- [8]. Eastman, J. A., Choi, S. U. S., Li, S., Yu, W., and Thompson, L. J. (2001). Anomalous increased effective thermal conductivities of ethylene glycol-based nanofluids containing copper nano-particles. *Applied Physics Letters*, 78, no.6, 718720.
- [9]. Fatunmbi, E. O., Ogunseye, H. A., Sibanda, P. (2020). Magnetohydrodynamic Micropolar Fluid Flow in a Porous Medium with Multiple Slip Conditions. *International Communication in Heat and Mass Transfer*. 115, 104577.
- [10]. Hakeem, A. K. A., Bhose, G., Sait, M. Y. A., Nagaraj, V. G., Muhammad, M. R. (2017).
- [11]. Nonlinear Studies on the Effect of non-Uniform Heat Generation/Absorption on Hydromagnetic Flow of Nanofluid Over a Vertical Plate. *Journal of Nonlinear Analysis, Modelling and Control*. Vol. 22, No.1, 1-16. <http://dx.doi.org/10.15388/NA.2017.1.1>. ISSN 1392-5113.
- [12]. Hamid, A. K., Azmi, W. H., Mamat, R., Usri, N. A. and Najafi, G. (2015). Investigation of Al₂O₃ Nanofluid viscosity for different water/EG mixture based. *Energy Procedia* 79(2015), 354-359. 2015 International conference on alternative Energy in Developing countries and Emerging Economics. www.sciencedirect.com
- [13]. Islam, S., Khan, A., Kuman, P., Alrabaiah, H., Shah, Z., Khan, W., Zubair, M., and Jawad, M.
- [14]. (2020). Radiative Mixed Convection Flow of Maxwell Nanofluid Over a Stretching Cylinder with Joule Heating and Heat Source/Sink Effects. *Science Reports*, 10, 1-18.
- [15]. Khan, A., Shah, Z., Alzahrani, E., and Islam, S. (2020). Entropy Generation and Thermal Analysis for Rotating Motion of Hydromagnetic Casson Nanofluid Past a Rotating Cylinder with Joule Heating Effect. *International Communication in Heat Mass Transfer*, 119, 104979.
- [16]. Khan, A., Kumam, W., Khan, I., Saeed, A., Gul, T., Kumam, P., Ali, I. (2021). Chemically Reactive Nanofluid Flow Past a Thin Moving Needle with Viscous Dissipation, Magnetic Effects and Hall Current. *PLoS ONE*, 16, e0249264. [CrossRef] [PubMed].
- [17]. Loganathan, K. and Rajan, D. (2020). An Entropy Approach of Williamson Nanofluid Flow with Joule Heating and Zero Nanoparticle mass flux. *Journal of Thermal Analysis and Calorimetry*, Volume 141, Number 6. Page 2599-2612.
- [18]. Nadeem, S., Khan, M., Abbas, N. (2020). Transportation of Slip Effects on Nanomaterial Micropolar Fluid Flow Over Exponentially Stretching. *Alexandria Engineering Journal*; 59, 3443-3450.
- [19]. Omamoke E., Amos E., and Bunonyo K. W. (2020). Radiation and heat source effects on MHD free convective flow over an inclined porous plate in the presence of viscous dissipation. *American Journal of Applied Mathematics*, 8(4), 190-206.
- [20]. Patil, P. M., Kulkarni, M., and Hiremath, P. (2019). Effects of Surface Roughness on Mixed Convection Nanofluid Flo Past an Exponentially Stretching Permeable Surface. *Chinese Journal of Physics-Taipei*-64(2). DOI: 10.1016/j.cjph.2019.12.006.
- [21]. Sheremet, M. A., and Pop, L., and Shenoy, A. (2015). Unsteady free Convection in a Porous Open wavy cavity filled with a nanofluid using Buongiorno's mathematical Model. *International Communications in Heat and Mass Transfer* 67. DOI: 10.1016/j.icheatmasstransfer.2015.07.007.
- [22]. Sheremet, M. A., Oztop, H. F., Pop, I., and Al-Salem, K. (2016). MHD free convection in a wavy open porous tall cavity filled with nanofluids under an effect of corner heater. *International Journal of Heat and Mass Transfer*. Published by Elsevier Science. Vol.03, pp.955-964, J. ISSN:0017-9310. DOI: 10.1016/j.ijheatmasstransfer.2016.08.006.
- [23]. Waini, I., Ishak, A., and Pop, I. (2020). Mixed Convection Flow Over an Exponentially Stretching/Shrinking Vertical Surface in a Hybrid Nanofluid. *Alexander Engineering Journal*. 59,1881-1891.

Emeka Amos, et. al. "Hydromagnetic Nanofluid Flow over an Exponentially Stretching Sheet in the Presence of Radiation and Nonuniform Heat Generation/Absorption." *IOSR Journal of Mathematics (IOSR-JM)*, 18(1), (2022): pp. 31-43.